Equilibrium and transport properties of CO_2+N_2O and CO_2+NO mixtures. A molecular simulation and equation of state modelling study.

V. Lachet[a,*], B. Creton[a], T. de Bruin[a], E. Bourasseau[b], N. Desbiens[b], Ø. Wilhelmsen[c], M. Hammer[c]

[a] IFP Energies nouvelles, 1 et 4 avenue de Bois Préau, 92852 Rueil-Malmaison, France
[b] CEA, DAM, DIF, F-91297 Arpajon, France
[c] SINTEF Energy Research, Kolbjørn Hejes vei 1A, 7465 Trondheim, Norway

Abstract
In the present study, the thermodynamic behaviour and transport properties of CO_2+N_2O and CO_2+NO mixtures have been investigated using molecular simulation and equation of state modelling. Molecular simulations were based on Monte Carlo and Molecular Dynamics calculations using force fields calibrated from pure component properties and no adjustment of mixture properties was performed. Original force fields were proposed for N_2O, NO and N_2O_2 molecules. Special attention must be paid when studying nitric oxide containing systems because this compound can exist as a mixture of monomers (NO) and dimers (N_2O_2) under certain pressure and temperature conditions. Liquid-vapour coexistence properties of the reacting NO-N_2O_2 system were thus first investigated using combined reaction ensemble and Gibbs ensemble Monte Carlo methods. Using the new force fields proposed, phase compositions, phase densities and phase viscosities were determined for CO_2+NO_x mixtures. Due to the strong similarities between carbon dioxide and nitrous oxide ($T_c(CO_2)$ = 304.21 K; $T_c(N_2O)$ = 309.57 K; $P_c(CO_2)$ = 7.38 MPa; $P_c(N_2O)$ = 7.24 MPa), the obtained thermodynamic and transport properties for a CO_2+N_2O mixture with 10 mol% of N_2O are similar to pure CO_2 properties in the whole range of studied temperatures (273 – 293 K), in agreement with available experimental data. Calculations of CO_2+NO equilibrium and transport properties were also performed at three different temperatures in the range of 253 – 273 K. At these temperatures, only the monomer form of the nitric oxide (NO) has to be accounted for. The performed calculations are pure predictions since no experimental data are available in the open literature for this system. For a mixture containing 10 mol% of NO, the simulation results show a decrease of the liquid densities and viscosities of 9% and 24% with respect to corresponding pure CO_2 values, respectively. The new pseudo-experimental data generated in this work were finally used to calibrate binary interaction parameters required in standard cubic equations of states. Both Peng-Robinson and Soave-Redlich-Kwong equations of state have been considered and after the regression, they display a decent match with experimental and pseudo-experimental data of the vapour-liquid equilibrium for the two studied mixtures.

Keywords: CO_2 capture and storage; VLE data; Viscosity; Molecular simulation; Equation of state.

1. Introduction

In Carbon dioxide Capture and Storage (CCS) operations, the captured CO_2 stream from industrial installations is not a pure CO_2: it contains some associated compounds, also called

* Corresponding author. Tel.: + 33 1 47 52 61 22; fax: + 33 1 47 52 70 25.
E-mail address: veronique.lachet@ifpen.fr

contaminants, such as N_2, O_2, Ar, SO_x, NO_x... [1]. This mixture of gases may have significantly different thermo-physical properties as compared to a pure carbon dioxide. This may have impacts on the different stages of the CCS chain: capture, transportation, compression, injection and storage. To globally account for this impact and for a precise specification of maximal amounts of contaminants that can be tolerated in CO_2 flues, further investigations are strongly desired. Obtaining accurate knowledge of the thermodynamic and transport behaviour of CO_2+contaminant mixtures is part of the studies that are necessary in order to develop optimized carbon dioxide capture and storage processes. Some of these CO_2+contaminant mixtures, like CO_2+O_2 and CO_2+N_2 for instance, have already been studied over a large range of pressures and temperatures. A comprehensive review of available equilibrium and transport properties of CO_2+contaminant mixtures is proposed in two recent papers by Li and co-workers [2,3]. In the case of CO_2+NO_x mixtures, data are very scarce or nonexistent. As far as the CO_2+NO mixture is concerned, to the best of our knowledge, no experimental data are available in the literature. Concerning liquid-vapour equilibrium of the CO_2+N_2O mixture, some experimental data are reported in the works of Caubet [4,5], of Cook [6] and of Rowlinson [7]. These liquid-vapour equilibrium data cover some temperatures between 277 and 311 K and pressures between 3.5 and 7.5 MPa. Excess properties of CO_2+N_2O mixtures are also reported in the literature: excess enthalpies and excess volumes have been measured by Wormald [8] and by Cabanas [9] for both liquid and vapour CO_2+N_2O mixtures. Concerning CO_2+N_2O viscosities, some values at atmospheric pressure are reported by Kestin [10] for temperatures in the range 298 – 473 K and for N_2O contents of 31 and 65 mol%.

The objective of the present work is to compensate the lack of experimental data by generating so-called pseudo-experimental data based on numerical experiments using molecular simulation calculations. Molecular simulation is a widespread technique which consists of performing a detailed simulation of microscopic systems and of calculating appropriate averages in order to derive macroscopic fluid properties. Phase compositions, phase densities and phase viscosities of CO_2+N_2O and CO_2+NO mixtures have been determined using Monte Carlo and/or Molecular Dynamics simulations for temperatures in the range 253 – 293 K. These calculations have been performed using force fields based on pure component properties and no adjustment on mixture properties was required. In order to achieve accurate predictions, new optimized force fields were proposed for both nitrous oxide and nitric oxide molecules. Finally, standard cubic equations of states have been optimized in order to reproduce the thermodynamic behaviour of both mixtures. Available experimental data or our new simulated data were taken into account in the parameter regression procedure.

This article is organized as follows. In Section 2, the description of the simulation methods and expressions used to compute intermolecular potential energy are given. The new force fields developed to model N_2O and NO molecules are presented in Section 3.1 where they are tested with respect to their ability to reproduce thermodynamic and transport properties of pure compounds. In Sections 3.2 and 3.3, we present and discuss the simulated results obtained for the two studied binary mixtures. Section 3.4 is devoted to the calibration of standard thermodynamic models. This paper ends with a fourth section which contains our conclusions.

2. Simulation methods

2.1. Monte Carlo method

The liquid–vapour equilibrium data of pure compounds and binary mixtures were obtained with Monte Carlo (MC) simulations using the GIBBS Monte Carlo code [11]. These simulations were performed in the Gibbs NVT ensemble (constant number of particles N, constant total volume V and constant temperature T) or Gibbs NPT ensemble (constant number of particles N, constant pressure P and constant temperature T) [12]. In such simulations, the two phases are simulated in individual boxes without an explicit interface, and particle transfers between boxes are performed in order to ensure phase equilibrium. In most cases, the following Monte Carlo moves were used in order to sample the configurational space:

- internal moves (rigid body translation and rotation of a molecule),
- volume changes (opposite volume changes $+\Delta V$ and $-\Delta V$ are applied to the two boxes in the case of Gibbs NVT simulations in order to keep the total volume constant),
- transfers between phases based on the pre-insertion bias. This pre-insertion bias algorithm, used to improve the efficiency of the sampling [13], involves two steps. The first step consists in the selection of a suitable location for inserting a new molecule by testing several places with a simple Lennard-Jones particle. The second step involves the test of several molecular orientations with the centre of mass at the location selected in the first step.

In the case of NO-containing systems, one additional Monte Carlo move, the reaction move, has been used in order to account for the possible dimerization of two NO molecules into N_2O_2. These particular simulations are described in section 3.1.2. For all other studied systems, the selected probabilities for the different Monte Carlo moves are 0.3 for translations, 0.3 for rotations, 0.395 for transfers, and 0.005 for volume changes. A total number of 500 to 800 molecules has been considered in our MC simulations, depending on the proximity of the studied temperature to critical temperatures of involved species. A total number of at least 50 million Monte Carlo iterations have been performed for each studied condition.

For the different studied molecules, the molar enthalpy of vaporization was computed at different temperatures as the difference between the average molar enthalpies of the vapour and liquid simulation boxes. The statistical uncertainties of the calculated phase properties were estimated by the block averaging technique [14]. The statistical uncertainties on the molar enthalpy of vaporization are typically 2–3%. The saturated vapour pressure was computed using the Virial equation, and the associated statistical uncertainty was less than 5%. The average liquid density was generally determined with a statistical uncertainty of 1–2% for both pure compounds and mixtures, but higher values are found at near-critical temperatures as a result of larger fluctuations.

2.2. Molecular Dynamics

Properties such as the density and the dynamic viscosity have been calculated using Molecular Dynamics (MD) simulations with NEWTON, a MD code developed for flexible and rigid molecules [15]. In contrast to the MC procedure, MD simulations follow the time evolution of a molecular system by numerically integrating Newton's equations of motion. Simulations in the isobaric-isothermal ensemble (NPT) were performed to compute the density and the viscosity of the considered systems. Up to 1000 molecules were considered in our MD simulations. The velocity Verlet algorithm was used to integrate the equations of motion, with a time step of 1 fs. Practically, MD simulations were split in two parts: (i) one having a 0.2 ns length (2.10^5 steps) intended to the equilibration of the system, (ii) one with a 5 ns length (5.10^6 steps) that is dedicated to the calculation of the desired properties.

As described in previous works [16,17], the viscosity can be calculated either in the canonical ensemble (NVT) or in the isobaric-isothermal ensemble (NPT). The Einstein relation was employed to compute the viscosity η of systems of interest using the following expression

$$\eta = \frac{1}{20}\frac{V}{k_B T}\lim_{t\to\infty}\frac{d}{dt}\left[\sum_{\alpha}\left\langle \Delta P_{\alpha\alpha}^{T}(t)^2\right\rangle + 2\sum_{\alpha>\beta}\left\langle \Delta P_{\alpha\beta}(t)^2\right\rangle\right] \qquad (1)$$

where, α and β run over the three cartesian coordinates, k_B is the Boltzmann constant, V is the volume, T the temperature and $\Delta P_{\alpha\beta}$ denotes the displacement of the elements of the pressure tensor $P_{\alpha\beta}$.

2.3. Interaction potential and calculation procedure

All the molecules involved in this study have been considered to be rigid, thus no intramolecular energy has been accounted for. Only intermolecular energy has been calculated with the two following contributions: dispersion - repulsion and electrostatic.
Dispersion-repulsion energy between two force centres is represented as a function of their separation distance *r* with a Lennard-Jones (LJ) potential:

$$U_{LJ} = U_{rep} + U_{disp} = 4\varepsilon\left(\left(\frac{\sigma}{r}\right)^{12} - \left(\frac{\sigma}{r}\right)^{6}\right) \qquad (2)$$

In the case of binary interactions involving different force centres *i* and *j*, two combining rules have been used following requirements of intermolecular potentials. Lorentz-Berthelot combining rules are defined by:

$$\varepsilon_{ij} = \sqrt{\varepsilon_i\,\varepsilon_j} \qquad (3)$$

$$\sigma_{ij} = \frac{\sigma_i + \sigma_j}{2} \qquad (4)$$

The geometric combining rules are defined by:

$$\varepsilon_{ij} = \sqrt{\varepsilon_i\,\varepsilon_j} \qquad (5)$$

$$\sigma_{ij} = \sqrt{\sigma_i\,\sigma_j} \qquad (6)$$

Unless specified otherwise, Lorentz-Berthelot combining rules have been used to be consistent with previous studies [18-20].

Electrostatic energy is computed from the Coulomb law, assuming that the molecules bear electrostatic point charges:

$$U_{elec} = \frac{q_i\,q_j}{4\pi\varepsilon_0 r_{ij}} \qquad (7)$$

where q_i and q_j are two charges belonging to different molecules, r_{ij} is the distance separating the charges and ε_0 is the vacuum permittivity.

Numerical values of the involved parameters for all studied molecules, *i.e.* Lennard-Jones diameters, Lennard-Jones well depths and electrostatic charges, will be discussed and given in the following sections.

Calculation of intermolecular energy is made by applying periodic boundary conditions, following classical procedures of molecular simulations [14,21]. Lennard-Jones interactions

have been computed by applying a cut-off distance set to half of the box length. A standard long distance correction was used to account for interactions beyond the cut-off distance. The calculation of electrostatic interactions has been done using the Ewald summation method with 7 vectors in each space direction and a Gaussian width set to $2\pi/L$, where L is the size of the simulation box.

3. Results

3.1. New interaction potentials for N_2O and NO

3.1.1. Model for nitrous oxide

Two intermolecular potentials suitable for liquid-vapour equilibrium studies are available in the literature to model nitrous oxide (N_2O) molecules. Both are based on Lennard-Jones plus point charge models. The first one has been proposed by Costa Gomes et al. in 2006 [22] and the second one by Hansen et al. one year later [23]. The parameters of these two potentials are summarized in Table 1. The accuracy of the models can be evaluated from Fig. 1 to 3 where calculated equilibrium properties are compared to available experimental data. Note that for simulations employing the Costa Gomes force field geometric mixing rules are used for both the size and the energy parameters, whereas classical Lorentz-Berthelot combining rules are used in the Hansen potential. Although both models have been fitted to vapour-liquid equilibrium data, the degree of agreement between experimental and simulated values is not fully satisfying. The first step of the present work was thus the determination of a new interaction potential for nitrous oxide that allows a better quantitative agreement between simulation and experiment over a wide range of temperatures. In the proposed model, the N-N and N-O distances, as well as the N-N-O angle, were fixed to their experimental values [24] (lN_1-N_2 = 1.1282 Å; lN_2-O = 1.1842 Å and N_1-N_2-O = 180°). Three Lennard-Jones and three point charges have been considered located on the three atoms of the molecule. In order to achieve a good degree of accuracy, the two nitrogen atoms of the molecule have been modelled by two different force centres as previously proposed by Hansen et al. The point charges and the Lennard-Jones parameters of the two nitrogen atoms and of the oxygen atom have been optimized using the following objective function [25]:

$$F = \sum_{i=1}^{n} \frac{\left(X_i^{sim} - X_i^{\exp}\right)}{S_i^2}, \qquad (8)$$

where the sum runs over saturation properties (density, vaporization enthalpy and saturated vapour pressure), $X_i^{\exp}$ stands for experimental measurements, X_i^{sim} denotes the associated computed properties, and S_i are the estimated statistical uncertainties on X_i^{sim} calculated by the block averaging technique. The minimization of the F function was realized as described in previous works [13,26] using a first-order Taylor expansion of thermodynamic properties versus potential parameters. For this purpose the gradient of F versus the potential parameters was obtained by a fluctuation method [11,27]. It was found that any direct optimization attempt involving more than two parameters failed to converge towards a better optimum, which is a known result from statistical uncertainties in a context where some parameter variations may compensate for each other (this is for instance the case between the Lennard Jones diameters of oxygen and nitrogen atoms). Thus the optimization has been performed by successive steps using 1D- and 2D-subspaces of the full parameter set. Moreover, due to the similar electronic environments of the N_1 and the O atoms in the N_2O molecule, identical

charges on these two atoms have been imposed. The optimization procedure leads to the charges and Lennard-Jones parameters presented in Table 1.

Table 1: Intermolecular potential parameters for N_2O.

Model	**Site**	**ε/k_B (K)**	**σ (Å)**	**q (e)**	**Bond length (Å)**
N_2O (this work)	N1	78.107	3.116	-0.3400	l_{N1-N2} = 1.1282
	N2	34.647	2.927	0.6800	l_{N2-O} = 1.1842
	O	65.891	3.044	-0.3400	
N_2O (Costa Gomes et al. [22])	N1	56.527	3.150	-0.2497	l_{N1-N2} = 1.1280
	N2	56.527	3.150	0.5159	l_{N2-O} = 1.1840
	O	78.177	3.050	-0.2662	
N_2O (Hansen et al. [23])	N1	79.167	3.120	-0.3630	l_{N1-N2} = 1.1282
	N2	27.000	2.800	0.7130	l_{N2-O} = 1.1842
	O	79.000	3.050	-0.3500	

Fig. 1 to 3 compare experimental data and results obtained by Monte Carlo simulations in the Gibbs NVT ensemble using the models of Costa Gomes, of Hansen and our new force field. The respective average absolute deviations for the densities, the vaporization enthalpies and the saturated vapour pressures are 2.6, 9.5 and 24.7% for Costa Gomes intermolecular potential, 0.9, 7.4 and 6.7% for Hansen intermolecular potential and 1.0, 3.5 and 5.8% for our intermolecular

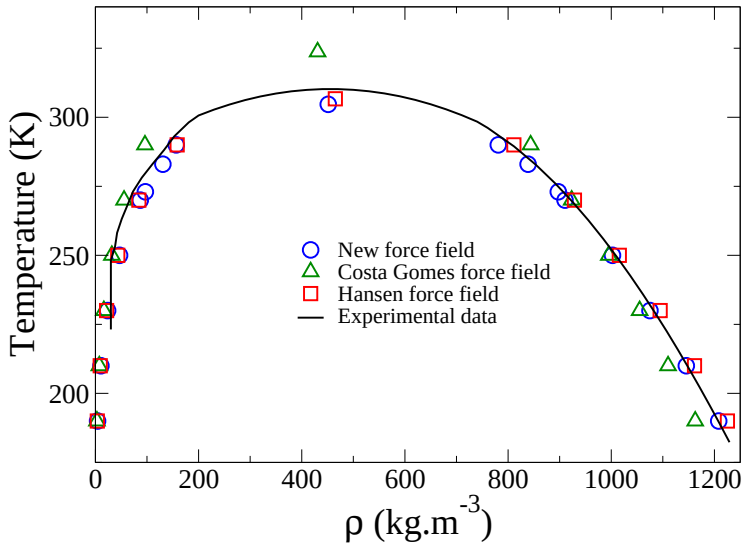

Fig. 1: Liquid-vapour coexisting densities of N_2O obtained by Monte Carlo simulations using the Hansen force field, the Costa Gomes force field and our new proposed force field. Experimental values shown for comparison are taken from the DIPPR data bank [28] for the liquid phase, and from the work of Quinn and Wernimont [29] for the vapour phase.

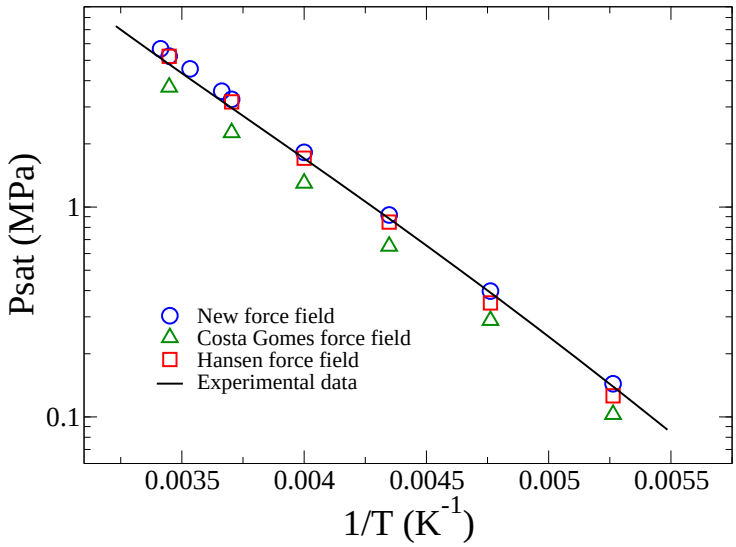

Fig. 2: Vapour pressures of N_2O obtained by Monte Carlo simulations using the Hansen force field, the Costa Gomes force field and our new proposed force field. Experimental values taken from the DIPPR data bank [28] are also shown for comparison.

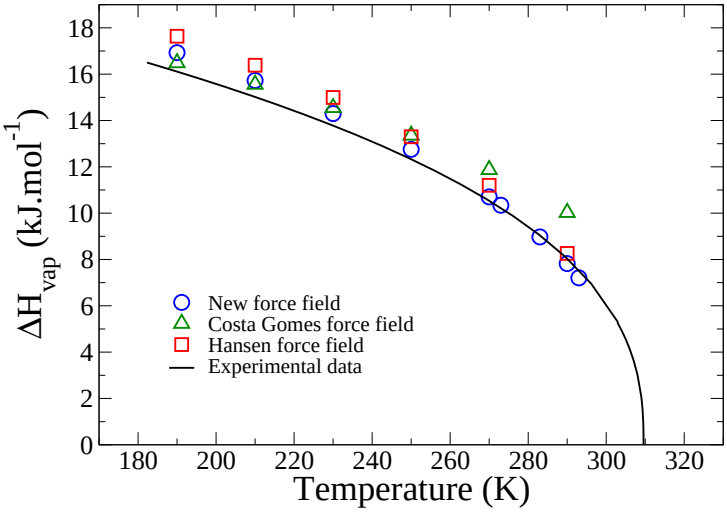

Fig. 3: Vaporization enthalpies of N_2O obtained by Monte Carlo simulations using the Hansen force field, the Costa Gomes force field and our new proposed force field. Experimental values taken from the DIPPR data bank [28] are also shown for comparison.

Fig. 4 presents the results obtained for nitrous oxide transport properties using MD simulations. The liquid viscosities are obtained with average absolute deviations from experiments of 35.2%, 22.3%, and 11.8% using the Hansen force field, the Costa Gomes force field, and our new force field, respectively. These comparisons show that our new force field allows a better accuracy also for transport properties compared to existing force fields. Note that densities obtained by MD are consistent with those computed using MC simulations.

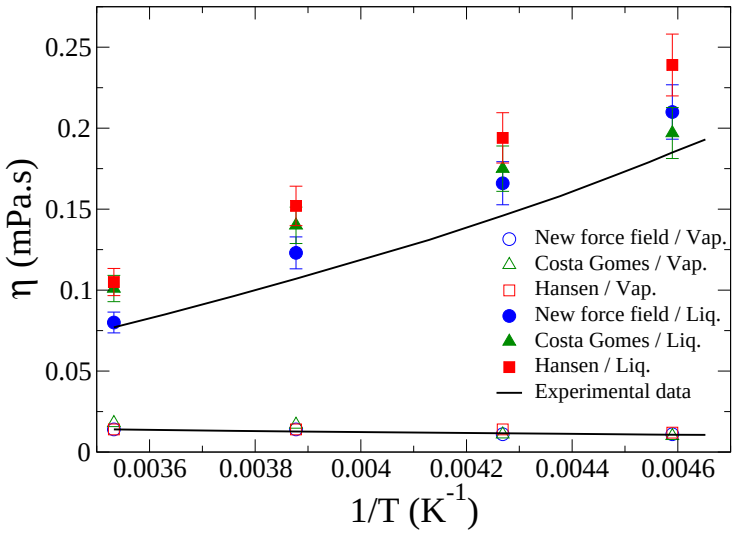

Fig. 4: Comparison of vapour and liquid viscosities of N_2O obtained by Molecular Dynamics simulations using the Hansen potential, the Costa Gomes potential and our new proposed potential. Experimental values are taken from the saturation properties of N_2O on the NIST website [30].

The accuracy of our force field in the vicinity of the critical point has also been investigated. Because of the large characteristic size of the density fluctuations, Gibbs Ensemble simulations cannot be performed in the close vicinity of the critical point. Therefore, the critical temperature T_c and the critical density ρ_c have been obtained by extrapolation from simulation points sufficiently far away from the critical point, assuming the following scaling law:

$$\rho^V - \rho^L = \gamma(T - T_c)^\beta \qquad (9)$$

where β is a characteristic universal exponent [31,32]. It is also assumed that the densities of the coexisting liquid and vapour obey the so-called law of rectilinear diameters:

$$\frac{\rho^V + \rho^L}{2} - \rho_c = \lambda(T - T_c) \qquad (10)$$

Practically, T_c and ρ_c have been regressed by a least square method minimizing the average deviation between the above equations and the simulated coexistence densities. Once these properties were obtained, the critical pressure was then estimated by extrapolating the Clapeyron plot (see Fig. 2) to $1/T_c$. The resulting critical coordinates, as well as the normal boiling point, are gathered in Table 2 where they are compared to experimental values taken from the DIPPR data base [28] and to simulated values obtained using the Costa Gomes and the Hansen models. A very accurate restitution of the critical point is obtained using our new force field with deviations from experiments of 1.6% for the critical temperature, 3.2% for the critical pressure and 0.1% for the critical density.

Table 2: N_2O critical coordinates and normal boiling temperature.

Model	**T_c (K)**	**P_c (MPa)**	**ρ_c (kg/m^3)**	**T_{eb} (K)**

N_2O (Exp)	309.57	7.24	451.88	184.67
N_2O (New force field)	304.70	7.47	451.32	183.33
N_2O (Costa Gomes [22])	323.69	7.69	430.71	189.05
N_2O (Hansen [23])	306.67	7.82	465.03	186.01

3.1.2. Model for nitric oxide

Systems containing nitric oxide are particularly challenging because this compound may exist as a mixture of monomers (NO: nitrogen monoxide or nitric oxide) and dimers (N_2O_2: dinitrogen dioxide). The composition of the NO-N_2O_2 equilibrium mixture depends on pressure and temperature conditions: the dimer is favoured at higher pressures and lower temperatures. The chemical equilibrium between N_2O_2 and 2 NO has been the subject of some experimental works [33-38] and of some theoretical investigations [34,39-41]. In the liquid state, this reaction has been studied by Smith et al. [33] and Guedes [34] who reported equilibrium constants from 110 K to 170 K. The mole fraction of dimers in saturated liquid nitric oxide was found to vary from more than 90% at 110 K down to ~40% at 170 K. From these studies, it can be inferred that nitric oxide is strongly associated in the saturated liquid phase at low temperatures and that this degree of association decreases with increasing temperatures. In the gas phase, dimerization can also occur but the fraction of associated molecules (N_2O_2) is very small. Equilibrium constants of the reaction in the gas phase along the saturation curve have been reported by Kohler et al. [42] showing a molar fraction of dimer in the vapour phase around 0.64 to 2.89% for temperatures in the range of 115 – 177 K. In addition to these studies of the $N_2O_2 \leftrightarrows 2NO$ chemical equilibrium, phase behaviours and phase properties of the NO-N_2O_2 reacting system have also been investigated in the literature from experimental studies [42-49] or from empirical modelling approaches [28,50]. Among others, we can cite Johnston and Giauque [44] who have reported heat capacity measurements from 14 K up to the boiling point, as well as vaporization enthalpies and vapour pressures.

In the present work, the vapour-liquid equilibrium of the NO-N_2O_2 reacting system has been simulated at a molecular level using simultaneously the reaction ensemble and the Gibbs NVT ensemble Monte Carlo methods [19,51]. The reaction ensemble Monte Carlo method (ReMC) [52,53] allows the study of chemically reacting mixtures. No detailed description of this ensemble is proposed here and we invite interested readers to investigate the papers cited above for more details. In comparison with classical Gibbs ensemble simulations, two additional constraints are applied:

• The number of atoms is fixed for each atom type, so the number of different molecules in the system is controlled by the chemical equation which defines the chemical equilibrium:

$$\sum_{i=1}^{s} \nu_i a_i = 0 \qquad (11)$$

where ν_i is the stoichiometric coefficient of chemical species *i*.

For example, $2NO \leftrightarrows N_2O_2$.

• The sum of chemical potentials μ_i over the different molecular species implied in the chemical reaction, weighted by stoichiometric coefficients, is equal to zero:

$$\sum_{i=1}^{s} \nu_i \mu_i = 0 \qquad (12)$$

For example, $2\mu_{NO} = \mu_{N_2O_2}$.

In order to satisfy these constraints during the simulation, an additional Monte Carlo move is used: the reaction move. This move consists in firstly choosing a direction to perform the reaction, second in deleting a set of reactant molecules randomly chosen in the system, and finally inserting product molecules. In our case, the reaction move is

$2NO \rightarrow N_2O_2$

where two randomly chosen NO molecules are deleted and one N_2O_2 is inserted, or

$N_2O_2 \rightarrow 2NO$

where one N_2O_2 molecule randomly selected is deleted and two NO molecules are inserted. The acceptance probability of such Monte Carlo move can be found in reference [19], together with some details on its implementation in the GIBBS Monte Carlo software used in this study.

Table 3: Intermolecular potential parameters for NO.

Model	**Site**	**ε/k_B (K)**	**σ (Å)**
NO - Hirschfelder 1 [54]	NO	91.0	3.60
NO - Hirschfelder 2 [54]	NO	119.0	3.47
NO - Kohler [55]	NO	125.0	3.17
NO - New force field (this work)	NO	130.0	3.40

To model NO and N_2O_2 molecules, we have parameterized a force field that treats NO as a single Lennard-Jones sphere and N_2O_2 as a two-site Lennard-Jones molecule. The parameterization procedure we have used is similar to the one previously described for N_2O force field development. The accuracy of the new proposed force field is compared to those obtained using existing models available in the literature [54,55]. Since the dipole moment of NO is rather small, electrostatic forces are neglected by all these models. The parameters of these different intermolecular potentials are summarized in Table 3. In order to test these models, we have performed NVT ReMC GEMC simulations at different temperatures in the 120 - 160 K range and computed the phase diagram of the reactive NO-N_2O_2 system. To model N_2O_2 molecules, we have used two NO LJ sites separated by 2.237 Å; the individual LJ parameters for each NO site in the dimer being the same as those for the monomer. The standard Gibbs free energies of the reaction $2NO \leftrightarrows N_2O_2$ needed to perform the reaction moves during these simulations were calculated from the Gibbs free energies of formation of NO and N_2O_2 taken from the TRC (Thermodynamics Research Center) thermochemical tables [56]. The numerical values of these Gibbs free energies are gathered in Table 4. Tests of these potentials have been performed by calculating thermodynamic properties of the NO-N_2O_2 system along the saturation curve. The obtained results (coexistence densities, vaporization enthalpies and vapour pressures) are presented in Fig. 5, 6 and 7, where they are compared to experimental or modelling data given in the DIPPR database [28]. For vapour pressures, results of Lísal et al. [57] using the Kohler force field are also plotted in Fig. 7, showing a very good agreement with our data using the same model. For all studied properties,

significant deviations between DIPPR and simulated data are observed when using either potentials of Hirschfelder or the potential of Kohler. The degree of agreement is much more satisfying with our new force field. The temperature dependence of liquid densities and vaporization enthalpies is correctly described by this model, although it slightly overestimates the liquid density and the vaporization enthalpy at low temperature and underestimates them at higher temperatures in the vicinity of the critical point. The respective average absolute deviations for the densities, the vaporization enthalpies and the saturated vapour pressures are 3.3, 8.0 and 27.0%. Such results show that this model allows a reasonable agreement between simulation and experiment over a wide range of temperatures.

Table 4: Standard Gibbs free energy changes ($\Delta_r G°$) of the reaction $2NO \leftrightarrows N_2O_2$ at the temperatures studied using reaction ensemble Monte Carlo. These values were evaluated by means of the TRC thermochemical tables [56].

T (K)	120.00	130.00	140.00	150.00	160.00
$\Delta_r G°$ (kJ mol^{-1})	5.344	6.726	8.126	9.530	10.936

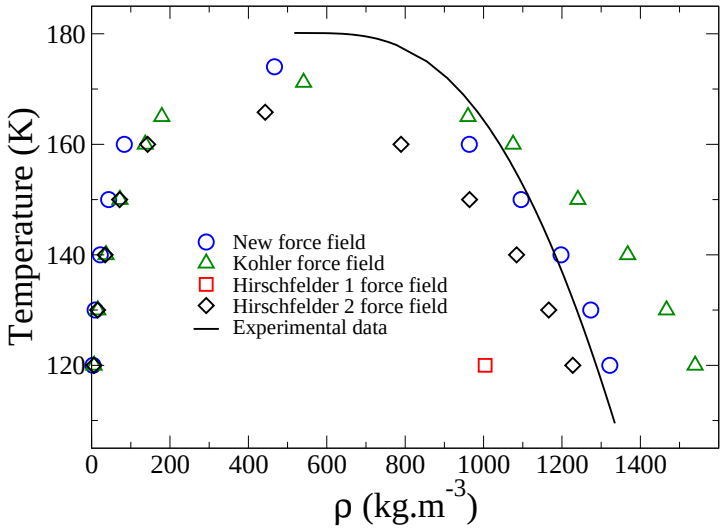

Fig. 5: Temperature dependence of density in the liquid-vapour coexistence region of the NO-N_2O_2 system. The line represents the recommended values of the DIPPR data bank [28] whereas symbols represent our Monte Carlo simulation results obtained using different interaction potentials to model the NO and N_2O_2 molecules.

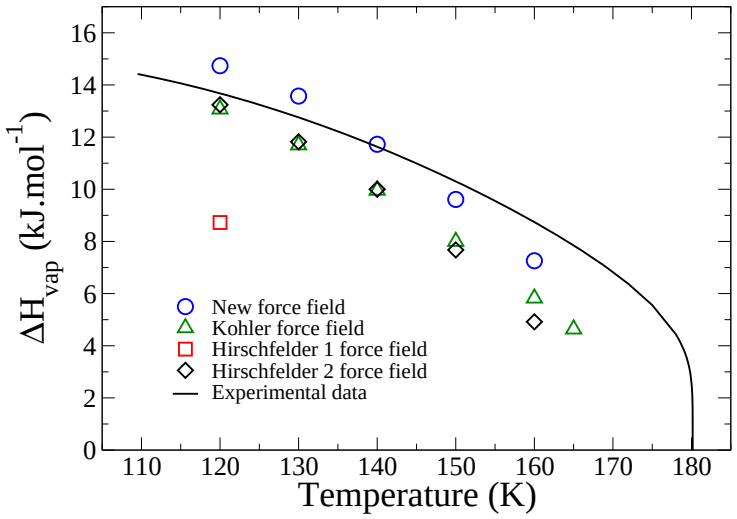

Fig. 6: Temperature dependence of vaporization enthalpies in the liquid-vapour coexistence region of the NO-N_2O_2 system. The line represents the recommended values of the DIPPR data bank [28] whereas symbols represent our Monte Carlo simulation results obtained using different interaction potentials to model the NO and N_2O_2 molecules.

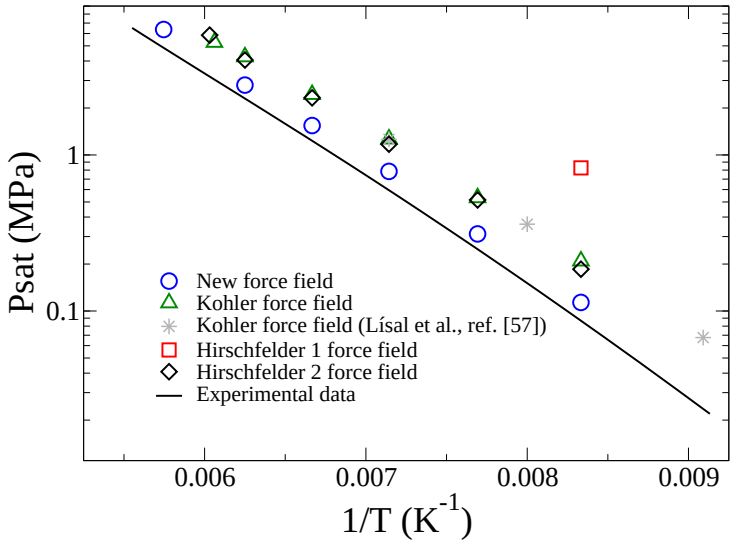

Fig. 7: Inverse temperature dependence of pressure in the liquid-vapour coexistence region of the NO-N_2O_2 system, in logarithmic scale. The line represents the recommended values of the DIPPR data bank [28] whereas symbols represent our Monte Carlo simulation results obtained using different interaction potentials to model the NO and N_2O_2 molecules. Results of Lísal et al. [57] using the Kohler force field are also shown for comparison.

The NO-N_2O_2 critical point coordinates (T_c, ρ_c and x_c) have been approximated by the use of extended scaling laws [11]:

$$\rho_{\varphi} = \rho_c + \lambda(T_c - T) + \varepsilon\frac{\gamma}{2}(T_c - T)^{\beta}$$

$$x_{\varphi} = x_c + \left(\lambda_1 - \varepsilon\frac{\lambda_2}{2}\right)(T_c - T) - \varepsilon\frac{\mu}{2}(T_c - T)^{\beta} \qquad (13)$$

where $\varepsilon = 1$ for the liquid phase (φ = liq) and $\varepsilon = -1$ for the vapour phase (φ = vap). T_c, ρ_c, x_c (critical coordinates) and λ, λ_1, λ_2, γ, μ (adjustable coefficients) are regressed by a least square method from a set of coexistence points (T, x_{liq}, x_{vap}, ρ_{liq}, ρ_{vap}) below the critical point. The critical pressure was then estimated by extrapolating the Clapeyron plot (see Fig. 7) to $1/T_c$. The resulting critical coordinates, obtained using the different studied force fields, are gathered in Table 5 where they are compared to experimental values taken from the DIPPR data base [28].

Table 5: Nitric oxide critical coordinates.

Model	**T_c (K)**	**P_c (MPa)**	**ρ_c (kg/m^3)**	**x_c (N_2O_2)**
Simulation (New force field)	174.03	6.37	466.60	0.03
Simulation (Hirschfelder 2 force field [54])	165.80	5.86	442.88	0.06
Simulation (Kohler force field [55])	171.19	7.64	540.86	0.04
DIPPR data	180.15	6.48	517.35	-

We have also compared the fractions of dimers in the saturated liquid phase given by the different studied models. Results are shown in Fig. 8 together with the experimental point of Smith [33] obtained by measurements of magnetic susceptibility. Fig. 8 shows nearly complete dimerization at low temperatures. Further, the degree of dimerization decreases with increasing temperature and at $T > T_c$, the system becomes monomeric. For the vapour phase at a pressure of 0.1 MPa and a temperature of 121.40 K we obtain, using our new model, a mole percent of monomers of 99.6%, which is in agreement with both Guggenheim's estimate based on analysis of second Virial coefficient data [58] and Turner's estimate based on Monte Carlo simulations [59]. To assess the possible effect of pressure on the degree of dimerization, one simulation of the NO-N_2O_2 system has been conducted in the monophasic liquid region at 253.15 K and 12.0 MPa, showing a mole fraction of monomers of 99.8%.

This study shows that our simulations are consistent with data available in the literature for both the liquid and the gas phases. The obtained results also show that for temperatures above the critical temperature of the NO-N_2O_2 system (T_c exp = 180.15 K), associations have disappeared and only the monomer form (NO) has to be accounted for.

Fig. 9 illustrates the results obtained for the transport properties of the NO-N_2O_2 system using MD simulations. The degree of dimerization for each studied temperature was taken from MC simulation results presented in Fig. 8, with a total number of 1000 NO particles. The viscosity calculations were thus performed at fixed chemical composition.

The liquid viscosities are obtained with average absolute deviations from experiments of 43.7%, 39.2%, and 22.0% using the Kohler force field, our new force field, and the Hirschfelder 2 force field, respectively. Such comparisons show that the Hirschfelder force field allows a better degree of accuracy for the liquid viscosity compared to Kohler and our new force fields, especially at low temperatures. However, considering both transport and thermodynamic properties, our new force field appears as the best compromise.

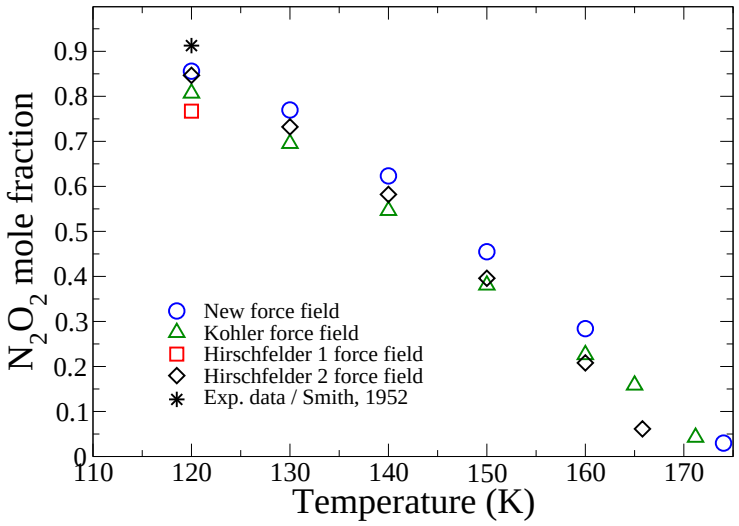

Fig. 8: Mole fraction of N_2O_2 as a function of temperature along the saturation line for the bulk liquid phase of the 2NO ⇆ N_2O_2 system from Monte Carlo simulations.

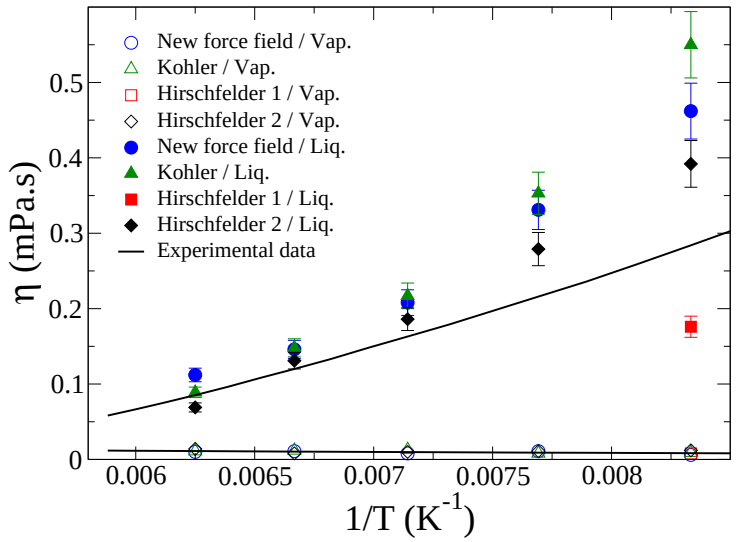

Fig. 9: Comparison of vapour and liquid viscosities of the NO-N_2O_2 system obtained by Molecular Dynamics simulations. Experimental values are taken from the saturation properties of NO on the NIST website [30].

3.2. Study of CO_2+N_2O mixtures

3.2.1. Vapour-liquid phase diagrams

To model CO_2 molecules, we have chosen the EPM2 rigid version of the force field proposed by Harris and Yung [60]. This force field, which involves three Lennard-Jones sites and three electrostatic charges, is known to represent the liquid-vapour coexistence data of pure CO_2 as well as phase diagrams of mixtures with other gases fairly well [18-20]. The parameters of this potential are given in Table 6. Note that Harris and Yung have developed their model using geometric combining rules for LJ sigma and epsilon. Nevertheless, in this work, Lennard-Jones parameters for the unlike interactions have been obtained using Lorentz-Berthelot rules. The use of an arithmetic combining rule for the calculation of sigma instead

of a geometric rule is not expected to have a significant impact on the simulation results since O and C atoms do not exhibit a substantial size difference (σO = 3.033 Å and σC = 2.757 Å). The use of an arithmetic combining rule leads to a cross diameter σCO equal to 2.895 Å, whereas a value of 2.892 Å is obtained with a geometric rule. Moreover, the paper of Nieto-Draghi and co-workers in 2007 shows that the combination of the Harris and Yung potential with the Lorentz-Berthelot rules allows a good restitution of both thermodynamic and transport properties.

Table 6: Intermolecular potential parameters for CO_2.

Model	Site	ε/k_B (K)	σ (Å)	q (e)	Bond length (Å)
CO_2 - EPM2 [60]	O	80.507	3.033	-0.3256	$l_{C\text{-}O}$ = 1.1490
	C	28.129	2.757	0.6512	
	O	80.507	3.033	-0.3256	

In order to increase the accuracy of the calculations performed for the CO_2+N_2O binary system, we have used the reaction Gibbs Ensemble Monte Carlo method proposed by Lísal et al. [61]. This approach uses a modified GEMC technique that treats the phase equilibrium as a special type of chemical reaction and incorporates knowledge of pure component vapour pressure data into the simulations. The present paragraph provides just a brief summary of the involved algorithm, the reader is referred to the paper of Lísal et al. for more details. From a practical point of view, this method is similar to the Gibbs Ensemble method except that the acceptance probabilities of particle transfers from one box to the other are modified according to the following equations:

$$P_{liq\to gas}^{acc}(a\to b)=\min\left(1,\Gamma_i\frac{N_{liq}V_{gas}}{(N_{gas}+1)V_{liq}}\exp(-\beta\Delta U)\right) \qquad (14)$$

$$P_{gas\to liq}^{acc}(a\to b)=\min\left(1,\frac{1}{\Gamma_i}\frac{N_{gas}V_{liq}}{(N_{liq}+1)V_{gas}}\exp(-\beta\Delta U)\right) \qquad (15)$$

where $\beta=1/(k_BT)$ and k_B is Boltzmann's constant, ΔU is the change in configurational energy, V_α is the volume of the simulation box α, and N_α is the total number of molecules in box α. In equations (14) and (15), the term Γ_i (i = CO_2 or N_2O) is given by:

$$\Gamma_i=\frac{P_{i,\exp}^{sat}}{P_{i,GEMC}^{sat}} \qquad (16)$$

with $P_{i,GEMC}^{sat}$ being the vapour pressure of component i calculated using standard GEMC and $P_{i,\exp}^{sat}$ the corresponding experimental value. If $\Gamma_i=1$, equations (14) and (15) correspond to standard GEMC simulations. In our simulations, we have used a constant Γ_i factor equal to 0.95 for the two involved compounds at the different studied temperatures. This choice is justified by the fact that the force fields used for N_2O and for CO_2 both lead to almost the same overestimate of vapour pressures whatever the temperature. All these simulations have

been performed at constant total volume and constant temperature. Note that no experimental information concerning the mixtures is required, making this approach totally predictive for mixture studies.

The phase envelopes of the CO_2+N_2O binary mixture have been calculated at three different temperatures: 273 K, 283 K and 293 K. These phase envelopes are presented in Fig. 10 together with experimental data of Cook measured at 293 K, 298 K and 303 K [6] and of Rowlinson measured at 283 K and 293 K [7]. All these temperatures are below the critical temperatures of both CO_2 and N_2O, thus none of the phase diagrams exhibits a critical point. Due to the strong similarities between carbon dioxide and nitrous oxide ($T_c(CO_2)$ = 304.21 K; $T_c(N_2O)$ = 309.57 K; $P_c(CO_2)$ = 7.38 MPa; $P_c(N_2O)$ = 7.24 MPa), the two-phase region is very narrow and very flat at all studied temperatures. Differences between the compositions of the liquid and the vapour phases at equilibrium are very small which means that the system may be considered to be azeotropic over the whole range of compositions. A good agreement between experimental and simulated data is obtained at 283 K and 293 K which validates our methodological approach. The numerical values obtained from the Monte Carlo simulations are gathered in Table 7. Fig. 11 presents the pressure-density diagrams obtained from our simulations.

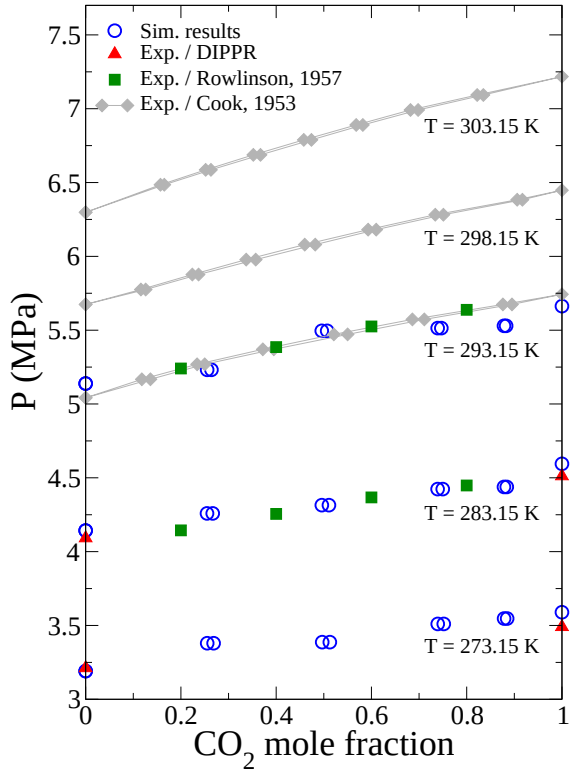

Fig. 10: Pressure-composition diagram of the CO_2+N_2O mixture at different temperatures. Experimental data at 283.15 K, 293.15 K, 298.15 K and 303.15 K are taken from Cook [6] and Rowlinson [7] whereas pure component vapour pressures at 273.15 K and 283.15 K are taken from the DIPPR data base [28].

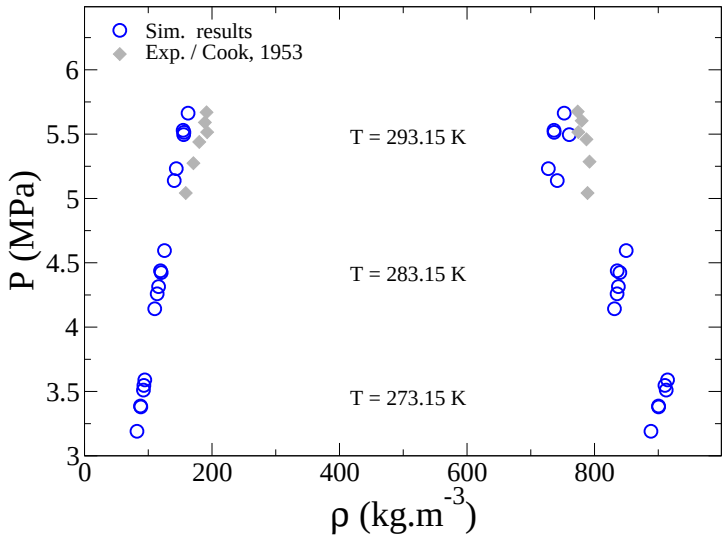

Fig. 11: Pressure-density diagram of the CO_2+N_2O mixture at different temperatures. Experimental densities have been taken from the work of Cook [6].

Table 7: Calculated vapour-liquid equilibrium pressures, compositions and densities for the CO_2+N_2O mixture at different temperatures.

T (K)	P (MPa)	x^{vap} (CO_2)	ρ^{vap} (kg/m^3)	x^{liq} (CO_2)	ρ^{liq} (kg/m^3)
293.15 K	5.14	0.000	140.73	0.000	741.55
	5.23	0.264	143.90	0.255	727.55
	5.50	0.507	155.52	0.496	760.40
	5.51	0.747	155.96	0.739	736.62
	5.53	0.883	154.75	0.878	736.49
	5.66	1.000	162.48	1.000	752.45
283.15 K	4.14	0.000	110.19	0.000	831.33
	4.26	0.267	113.94	0.255	835.39
	4.31	0.511	116.15	0.496	837.43
	4.42	0.750	120.34	0.739	839.75
	4.44	0.884	119.24	0.878	835.64
	4.59	1.000	125.41	1.000	849.76
273.15 K	3.19	0.000	82.29	0.000	888.59
	3.38	0.269	88.35	0.255	900.56
	3.39	0.513	87.86	0.497	900.40
	3.51	0.752	92.48	0.739	912.48
	3.55	0.885	93.12	0.879	910.45
	3.59	1.000	94.55	1.000	914.55

3.2.2. Densities and viscosities

In this section, we report results obtained using MD simulations for a CO_2+N_2O binary mixture containing 10 mol% of N_2O. The density and the viscosity of this mixture have been calculated at two temperatures: 283 K and 293 K. The obtained results are presented in Table 8 and illustrated in Fig. 12 and 13, together with experimental and simulated data for pure CO_2. Experimental data for pure CO_2 were extracted from the NIST website [30].

Densities simulated for pure CO_2 are in excellent agreement with respect to experimental data. When considering a CO_2+N_2O binary mixture containing 10 mol% of N_2O at 283 K and 293 K, Molecular Dynamics simulations lead to density values almost equal to the corresponding pure CO_2 values at the same temperatures. As far as the viscosity is concerned, data simulated for pure CO_2 show a reasonable agreement with respect to experimental data. Within the computed statistical uncertainties, the obtained viscosities for the mixture are similar to those calculated for pure CO_2 at the same temperature and pressure conditions.

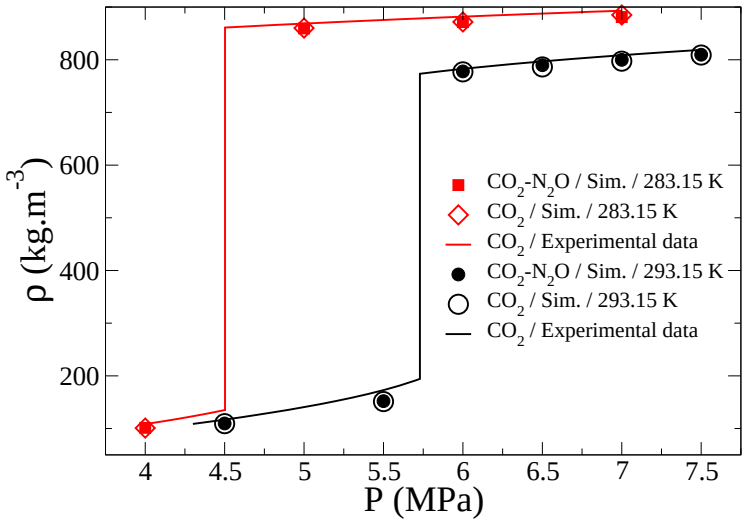

Fig. 12: Pressure-density diagram of the CO_2+N_2O mixture with 10 mol% of N_2O, at 283.15 K and 293.15 K. Experimental densities for pure CO_2 have been taken from the NIST website [30].

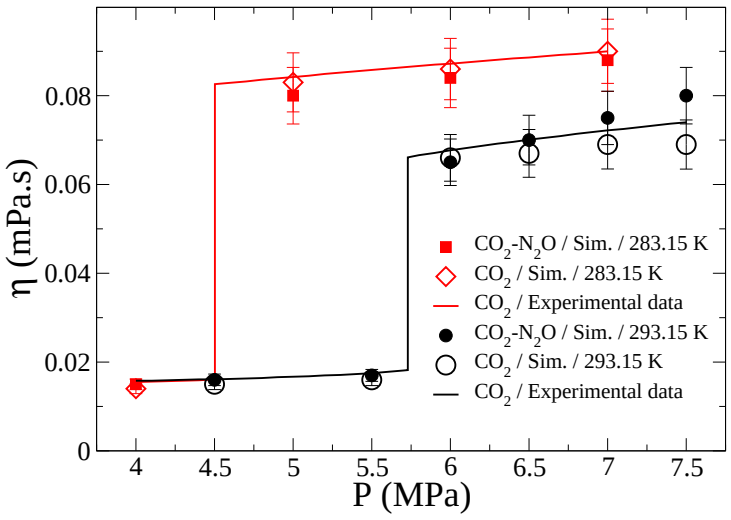

Fig. 13: Pressure-viscosity diagram of the CO_2+N_2O mixture with 10 mol% of N_2O, at 283.15 K and 293.15 K. Experimental viscosities for pure CO_2 have been taken from the NIST website [30].

Table 8: Molecular Dynamics simulation results computed for the CO_2+N_2O mixture with 10 mol% of N_2O. Simulated data obtained for the mixture are compared to experimental and simulated data for pure CO_2.

T (K)	P (MPa)	ρ (kg.m^{-3})	η (mPa.s)	ρ (kg.m^{-3})	err. (%)	η (mPa.s)	err. (%)	ρ (kg.m^{-3})	η (mPa.s)
		Exp. data for pure CO_2		Sim. data for pure CO_2				Sim. data for the CO_2+N_2O mixture	
293.15	4.5	116.9	0.016	109.3	-6.5	0.015	-6.7	109.6	0.016
293.15	5.5	172.9	0.018	151.1	-12.6	0.016	-7.5	152.0	0.017
293.15	6.0	782.7	0.068	777.0	-0.7	0.066	-2.8	777.8	0.065
293.15	6.5	796.8	0.070	786.4	-1.3	0.067	-4.0	789.6	0.070
293.15	7.0	808.6	0.072	797.3	-1.4	0.069	-4.6	799.8	0.075
293.15	7.5	818.7	0.074	808.9	-1.2	0.069	-6.5	809.5	0.080
283.15	4.0	108.4	0.015	100.9	-6.9	0.014	-10.3	101.2	0.015
283.15	5.0	868.6	0.084	860.0	-1.0	0.083	-1.3	859.5	0.080
283.15	6.0	881.8	0.087	871.7	-1.1	0.086	-1.0	871.5	0.084
283.15	7.0	893.1	0.090	884.9	-0.9	0.090	0.4	881.1	0.088

These calculations show that both thermodynamic and transport properties of CO_2+N_2O mixtures are similar to the properties of pure CO_2 in the whole range of studied temperatures, pressures and compositions. Such behaviour is reasonable due to the strong similarities between carbon dioxide and nitrous oxide in terms of molecular weights, vapour pressures and critical coordinates.

3.3. Study of CO_2+NO mixtures

3.3.1. Vapour-liquid phase diagrams

The phase envelopes of the CO_2+NO binary mixture have been calculated at three different temperatures: 253 K, 263 K and 273 K, using standard Gibbs NPT simulations. As discussed previously, nitric oxide is fully monomeric in this temperature range. The calculated phase envelopes are presented in Fig. 14 (pressure-composition diagrams) and Fig. 15 (pressure-density diagrams). The corresponding numerical values are gathered in Table 9. As expected, the extend of the two-phase region decreases as the temperature increases. The three studied temperatures are below the critical temperature of carbon dioxide (T_c = 304.21 K) and above the critical temperature of nitric oxide (T_c = 180.15 K), thus all phase diagrams exhibit a critical point. The coordinates of these critical points and the near-critical phase behaviour have been determined using extended scaling laws [11]. Obtained critical coordinates are: P_c = 11.48 MPa, ρ_c = 526.75 kg/m^3, x_c(NO) = 0.512 at 253 K; P_c = 11.21 MPa, ρ_c = 529.88 kg/m^3, x_c(NO) = 0.427 at 263 K and P_c = 10.95 MPa, ρ_c = 515.18 kg/m^3, x_c(NO) = 0.351 at 273 K.

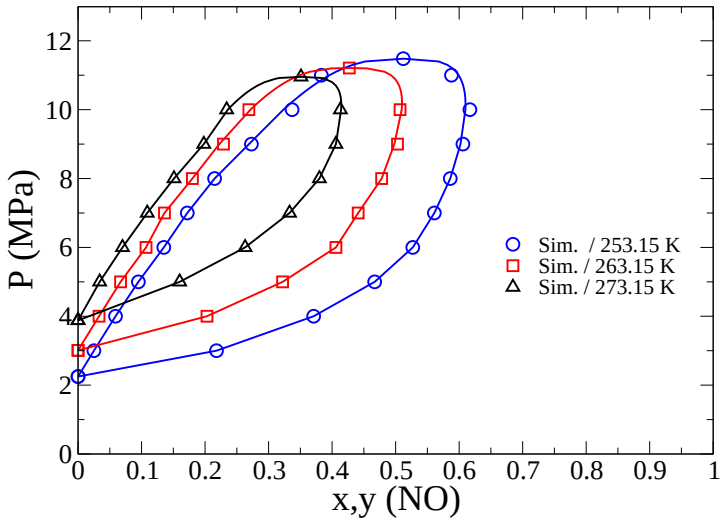

Fig. 14: Pressure-composition diagram of the CO_2+NO mixture at 253.15 K (blue), 263.15 K (red) and 273.15 K (black). The symbols represent the simulated results. The lines are guides for the eyes.

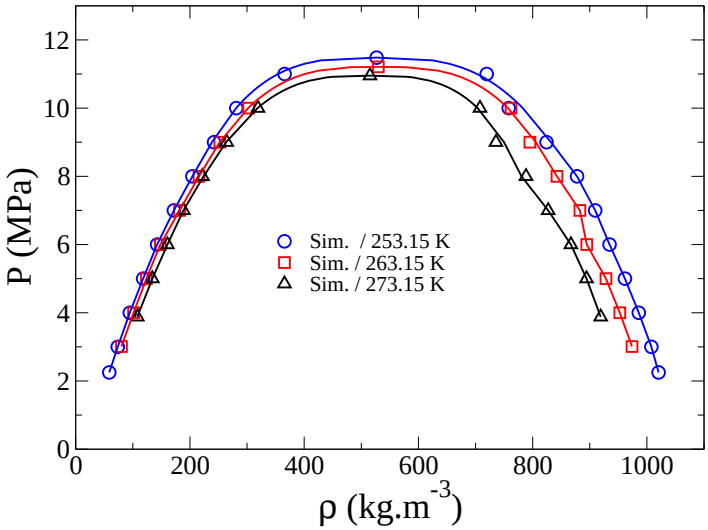

Fig. 15: Pressure-density diagram of the CO_2+NO mixture at 253.15 K (blue), 263.15 K (red) and 273.15 K (black). The symbols represent the simulated results. The lines are guides for the eyes.

Table 9: Calculated vapour-liquid equilibrium pressures, compositions and densities for the CO_2+NO mixture at different temperatures.

T (K)	P (MPa)	x^{vap} (NO)	ρ^{vap} (kg/m^3)	x^{liq} (NO)	ρ^{liq} (kg/m^3)
253.15 K	2.25	0.000	58.85	0.000	1020.5
	3.00	0.218	73.61	0.025	1007.8
	4.00	0.371	94.71	0.059	985.82
	5.00	0.467	118.09	0.095	961.58
	6.00	0.527	142.58	0.135	934.64
	7.00	0.561	171.90	0.172	909.53
	8.00	0.586	204.36	0.215	877.65

	9.00	0.606	242.19	0.273	824.31
	10.00	0.617	281.25	0.337	758.10
	11.00	0.588	365.77	0.383	719.47
	11.48*	0.512*	526.75*	0.512*	526.75*
263.15 K	3.01	0.000	80.22	0.000	973.92
	4.00	0.203	101.37	0.033	952.52
	5.00	0.322	123.86	0.067	928.29
	6.00	0.406	148.25	0.107	894.71
	7.00	0.441	181.94	0.136	882.70
	8.00	0.478	215.90	0.180	842.58
	9.00	0.503	252.28	0.229	795.19
	10.00	0.507	302.78	0.269	762.13
	11.21*	0.427*	529.88*	0.427*	529.88*
273.15 K	3.88	0.000	107.84	0.000	919.17
	5.00	0.160	134.21	0.034	894.28
	6.00	0.263	160.59	0.070	866.90
	7.00	0.333	188.68	0.109	827.16
	8.00	0.380	222.09	0.151	788.28
	9.00	0.406	264.35	0.198	735.64
	10.00	0.413	319.10	0.234	707.74
	10.95*	0.351*	515.18*	0.351*	515.18*

* Critical coordinates obtained using extended scaling laws.

3.3.2. Densities and viscosities

In this section, we report results obtained using MD simulations for a CO_2+NO binary mixture containing 10 mol% of NO. The density and the viscosity of this mixture have been calculated at two temperatures: 263 K and 273 K. As previously shown from MC simulation results, the nitric oxide is fully monomeric at these temperatures, and no N_2O_2 has been considered in the MD simulations. The obtained results are presented in Table 10 and illustrated in Fig. 16 and 17, together with experimental and simulated data for pure CO_2. Experimental data for pure CO_2 were extracted from the NIST website [30].

Densities and viscosities simulated for pure CO_2 are in excellent agreement with respect to experimental data. When considering a CO_2+NO binary mixture containing 10 mol% of NO at 263 K and 273 K, Molecular Dynamics simulations lead to liquid density values much lower than corresponding pure CO_2 values (about 9%). Similarly, the addition of 10 mol% of NO to CO_2 at 263 K and 273 K leads to a decrease of liquid viscosities of about 24% with respect to corresponding pure CO_2 viscosities.

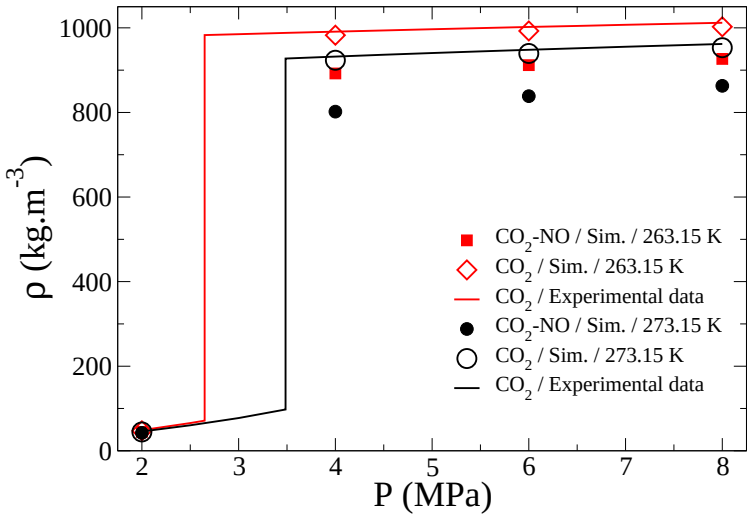

Fig. 16: Pressure-density diagram of the CO_2+NO mixture with 10 mol% of NO, at 263.15 K and 273.15 K. Experimental densities for pure CO_2 have been taken from the NIST website [30].

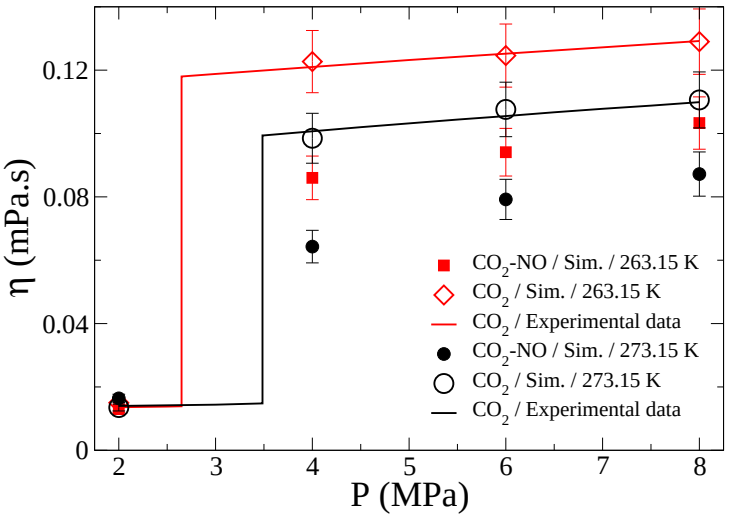

Fig. 17: Pressure-viscosity diagram of the CO_2+NO mixture with 10 mol% of NO, at 263.15 K and 273.15 K. Experimental viscosities for pure CO_2 have been taken from the NIST website [30].

Table 10: Molecular Dynamics simulation results computed for the CO_2+NO mixture with 10 mol% of NO. Simulated data obtained for the mixture are compared to experimental and simulated data for pure CO_2.

T (K)	**P (MPa)**	**ρ (kg.m^{-3})**	**η (mPa.s)**	**ρ (kg.m^{-3})**	**err. (%)**	**η (mPa.s)**	**err. (%)**	**ρ (kg.m^{-3})**	**η (mPa.s)**
		Exp. data for pure CO_2		Sim. data for pure CO_2				Sim. data for the CO_2+NO mixture	
273.15	2.0	45.6	0.014	44.5	-2.3	0.014	-3.7	42.3	0.016
273.15	4.0	932.1	0.101	923.4	-0.9	0.099	-2.2	801.9	0.064
273.15	6.0	948.2	0.106	939.5	-0.9	0.108	2.0	838.6	0.079

273.15	8.0	961.9	0.110	953.1	-0.9	0.111	0.6	862.9	0.087
263.15	2.0	48.8	0.014	47.3	-3.1	0.015	10.2	44.8	0.013
263.15	4.0	991.1	0.121	982.6	-0.9	0.123	1.4	892.2	0.086
263.15	6.0	1002.1	0.125	992.7	-0.9	0.125	-0.5	911.8	0.094
263.15	8.0	1012.0	0.129	1002.6	-0.9	0.129	-0.1	926.5	0.103

3.4. Optimization of thermodynamic models for CO_2+N_2O and CO_2+NO mixtures

The last part of the work is devoted to the calibration of standard cubic equations of state (EoS). Because of their simplicity and robustness, cubic EoS are often used to calculate the thermodynamic properties in the oil and gas process industry. Such EoS perform well for vapour-liquid equilibrium calculations and may perform well for densities, at least away from the critical region. Because they have few empirical parameters, they are easily fitted to new experimental data. In the present work, the available liquid-vapour experimental data or the pseudo-experimental data generated by molecular simulation have been used to regress binary interaction parameters for both Soave-Redlich-Kwong (SRK) and Peng-Robinson (PR) EoS for the CO_2+N_2O and CO_2+NO mixtures. Binary interaction parameters k_{ij} are required to calculate the attractive parameter a_{mix} and the co-volume b_{mix} of the mixture from a given mixing rule. In the present work, classical mixing rules have been used:

$$a_{mix} = \sum_{ij} z_i z_j \sqrt{a_i a_j}\,(1-k_{ij}), \qquad b_{mix} = \sum_{i} z_i b_i, \tag{17}$$

where the summations are over the mixture components i and where a_i, b_i, and z_i are the pure component attractive parameter, co-volume and molar fraction, respectively. For a given binary mixture and EoS, an unique binary interaction parameter has been regressed. The fitting of this interaction parameter has been performed by minimizing the objective function $Y(k_{ij})$, which is a sum over deviations for calculated data from experimental or pseudo-experimental data, with respect to k_{ij}:

$$Y(k_{ij}) = \left(\sum_{l=i,\,j} \sum_{r=1}^{N} \left[\left(x_{l,r}(k_{ij}) - x_{\mathrm{exp},l,r} \right)^2 + \left(y_{l,r}(k_{ij}) - y_{\mathrm{exp},l,r} \right)^2 \right] \right)^{\frac{1}{2}} \tag{18}$$

Here, the experimental data consists of N measurements (CO_2+N_2O) or data from molecular simulations (CO_2+NO) of the liquid compositions $x_{\mathrm{exp},r}$ and gas compositions $y_{\mathrm{exp},r}$, taken at a given point r in the pressure–temperature space. This is the same objective function as used by Wilhelmsen et al. [62]. $Y(k_{ij})$ is preferred compared to objective functions involving relative values, because molar fractions x and y may be small in terms of absolute values. A small absolute deviation may then result in a large relative deviation, and a biased regression. The performance of the EoS is measured by the absolute average deviation (AAD) of the liquid and gas compositions:

$$\mathrm{ADD}_x = \frac{1}{2N} \sum_{l=i,\,j} \sum_{r=1}^{N} \frac{\left| x_{l,r}(k_{ij}) - x_{\mathrm{exp},l,r} \right|}{x_{\mathrm{exp},l,r}} \tag{19}$$

and

$$\mathrm{ADD}_y = \frac{1}{2N}\sum_{l=i,\,j\,r=1}^{N}\frac{\left|y_{l,r}\left(k_{ij}\right)-y_{\mathrm{exp},l,r}\right|}{y_{\mathrm{exp},l,r}} \qquad (20)$$

The optimized parameters obtained for the two binary mixtures and the two studied EoS are gathered in Table 11, together with the corresponding performance.

Table 11: Optimized binary interaction parameters for the two studied mixtures and the two studied equations of state.

	CO_2+N_2O		CO_2+NO	
	SRK	PR	SRK	PR
k_{ij}	0.004	0.007	-0.119	-0.105
AAD_x	5%	1%	18%	19%
AAD_y	5%	3%	14%	14%

The phase envelopes of the CO_2+N_2O binary mixture as calculated by optimized cubic equations of state at 273 K, 283 K, 293 K, 298 K and 303 K are presented in Fig. 18 (pressure-composition diagrams) and Fig. 19 (pressure-density diagrams), together with the experimental data available in the literature and the Monte Carlo pseudo-experimental data obtained in the present work.

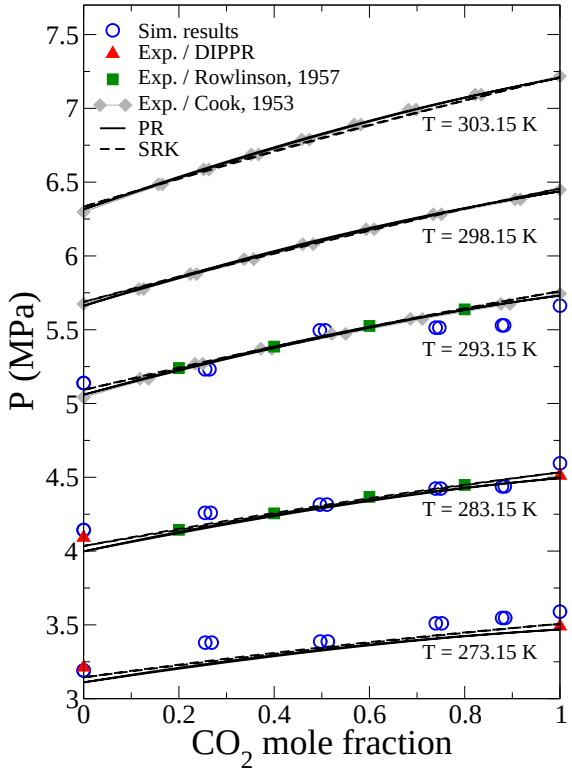

Fig. 18: Pressure-composition diagram of the CO_2+N_2O mixture at different temperatures; symbols: experimental or simulated results; solid lines: PR EoS results; dashed lines: SRK EoS results.

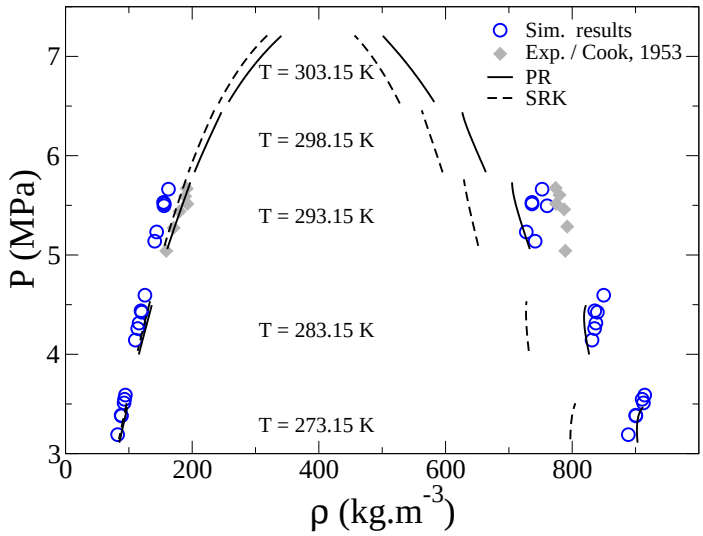

Fig. 19: Pressure-density diagram of the CO_2+N_2O mixture at different temperatures; symbols: experimental or simulated results; solid lines: PR EoS results; dashed lines: SRK EoS results.

The regression of binary interaction parameters for SRK and PR EoS based on experimental data allows a good description of the pressure-composition phase envelopes of the CO_2+N_2O mixture for all studied temperatures. For the two studied EoS, very small values of k_{ij} are obtained, which is reasonable since no significant cross interactions are expected in this system. Concerning coexisting densities, both EoS predict the densities well in the gas phase, but only the PR EoS allows a reasonable restitution of the liquid densities. SRK EoS underpredicts the liquid densities by more than 10%. Such behaviour was pointed out in recent work by Wilhelmsen et al. [62] involving different CO_2-containing systems. Note that no volume shift has been used to correct the obtained densities.

The phase envelopes of the CO_2+NO mixture calculated by the two cubic equations of state at 253 K, 263 K and 273 K are presented in Fig. 20 (pressure-composition diagrams) and Fig. 21 (pressure-density diagrams), together with the pseudo-experimental data from Monte Carlo simulations. In addition, the critical points of the CO_2+NO mixture at the three studied temperatures obtained from cubic equations of state are given in Table 12.

Table 12: Critical point predictions given by SRK EoS, PR EoS and Monte Carlo simulations for the CO_2+NO mixture at different temperatures.

	SRK EoS			PR EoS			Monte Carlo		
T (K)	P_c (MPa)	$x_{NO,c}$ (-)	ρ_c (kg/m^3)	P_c (MPa)	$x_{NO,c}$ (-)	ρ_c (kg/m^3)	P_c (MPa)	$x_{NO,c}$ (-)	ρ_c (kg/m^3)
253.15	13.7	0.562	510.2	13.6	0.554	559.1	11.48	0.512	526.8
263.15	13.2	0.483	491.4	13.1	0.476	537.5	11.21	0.427	529.9
273.15	12.4	0.395	471.1	12.3	0.388	513.2	10.95	0.351	515.2

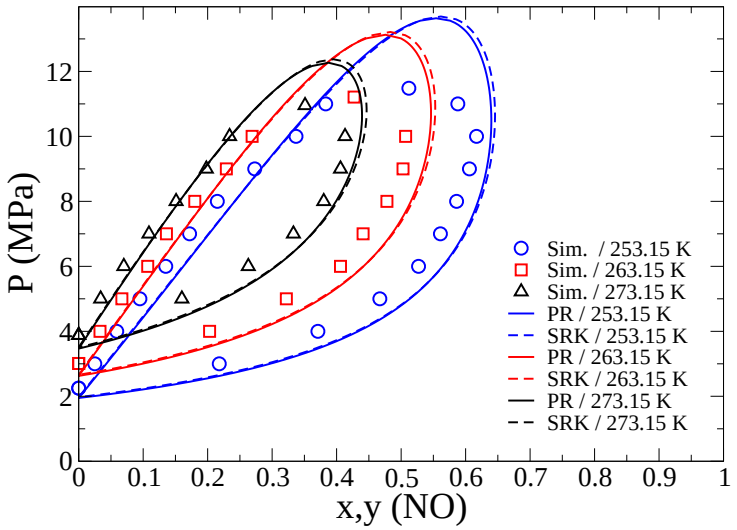

Fig. 20: Pressure-composition diagram of the CO_2+NO mixture at 253.15 K (blue), 263.15 K (red) and 273.15 K (black); symbols: simulated results; solid lines: PR EoS results; dashed lines: SRK EoS results.

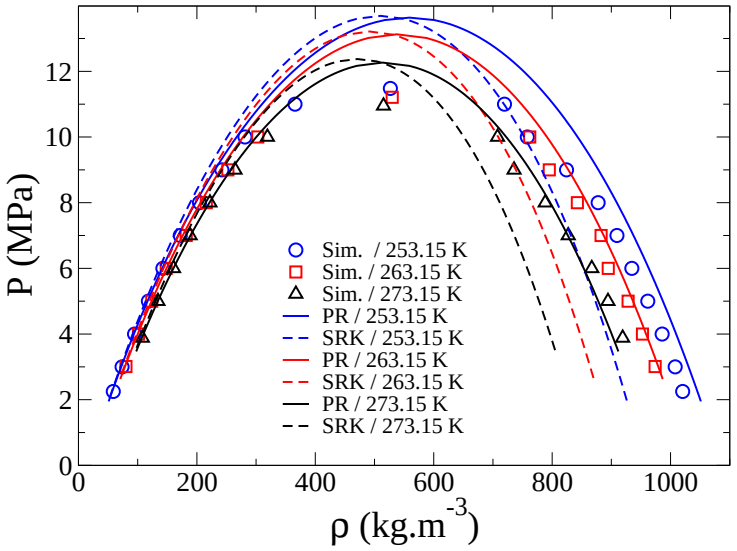

Fig. 21: Pressure-density diagram of the CO_2+NO mixture at 253.15 K (blue), 263.15 K (red) and 273.15 K (black); symbols: simulated results; solid lines: PR EoS results; dashed lines: SRK EoS results.

Fig. 20 shows that the largest deviations between the pseudo-experimental Monte Carlo data and the cubic equations of state may be found at large pressures in the vicinity of the critical region. This overprediction by standard cubic EoS of dew pressures close to the critical point was also found in a previous work [62] for two other CO_2+contaminant mixtures (CO_2+N_2 and CO_2+O_2) in a comparison with experimental data. In the present work with the CO_2+NO mixture, none of the cubic EoS displays any clear advantage over the other for the restitution of the pressure-composition curves. For density calculations however, Fig. 21 shows that the liquid densities calculated with the PR EoS are in better agreement with the Monte Carlo data compared to the values obtained with the SRK EoS. The same behaviour was already observed in the case of the CO_2+N_2O mixture. By comparing the data in Table 12, it is

evident that the critical coordinates given by the two cubic equations of state are similar, but very different from the critical coordinates given by Monte Carlo simulations. The deviations are largest for the critical pressures, which are on average 16% larger with the cubic equations of state than with Monte Carlo simulations. The critical composition exhibits only on average 10% deviation, while the predicted critical density from the cubic equations of state deviates 2% from the Monte Carlo simulations.

4. Conclusion

Original force fields for atomistic simulations have been proposed for N_2O, NO and N_2O_2 molecules, based on Lennard-Jones parameters fitted to experimental vapour-liquid equilibrium data. We have shown that thermodynamic and transport properties along the saturation curve of both nitrous oxide and nitric oxide can be well reproduced using these new models in Monte Carlo and Molecular Dynamics simulations. Studies have also been carried out on CO_2-containing mixtures at different temperatures in the range 253 – 293 K. Phase compositions, phase densities and phase viscosities were determined for CO_2+N_2O and CO_2+NO binary mixtures. In the case of CO_2+N_2O mixtures, the liquid-vapour phase envelopes calculated at 283 K and 293 K were compared with experimental data available in the literature. Experimental and simulation results appear in good agreement, allowing reliable and accurate predictions at other temperatures. In the case of CO_2+NO mixtures, the performed calculations are pure predictions since no experimental data are available in the literature for this system. The regression of binary interaction parameters for SRK and PR EoS based on the molecular simulation pseudo-experimental data or true experimental data allows good restitution of vapour-liquid equilibrium data for the two studied mixtures and for the two studied EoS. For the prediction of liquid densities in the two-phase area, PR EoS was much closer to the pseudo-experimental data than SRK EoS.

The present study shows that molecular simulations combined with equation of state modelling can play a significant role in the context of CO_2 storage operations where the degree of purity of the captured CO_2 is a key factor for transportation, injection and sequestration. This work illustrates how molecular simulations may be used as a tool to mitigate the lack of experimental data and improve engineering equations of state to enable process simulations where accurate, robust and computationally fast models are required.

List of symbols

a	cubic EoS attractive parameter (J m^3 mol^{-2})
b	cubic EoS co-volume (m^3 mol^{-1})
ΔH_{vap}	molar vaporization enthalpy (kJ mol^{-1})
F	objective function used in Eq. (8)
i, j	component i and j
k_B	Boltzmann's constant (J K^{-1})
k_{ij}	binary interaction parameter between components i and j
L	simulation box length (Å)
N	number of particles
P	pressure (MPa)
P_c	critical pressure (MPa)
Psat	saturated vapour pressure (MPa)
q_i	electrostatic charge (e)
r	separation distance (Å)
$P_{\alpha,\beta}$	element of pressure tensor (MPa)
S_i	statistical uncertainty on simulated property i

T	temperature (K)
T_c	critical temperature (K)
T_{eb}	normal boiling temperature (K)
U	configurational energy (J)
U_{LJ}	Lennard-Jones energy (J)
U_{elec}	electrostatic energy (J)
V	volume (m^3)
x	liquid phase mole fraction
X^{sim}, X^{exp}	simulated or experimental property
y	vapour phase mole fraction
Y	objective function used in Eq. (18)

Greek symbols

γ, λ, λ_1, λ_2, μ	adjustable coefficients used in Eqs. (9), (10) and (13)
β	characteristic universal exponent used in Eqs. (9) and (13)
ρ	density (kg m^{-3})
ρ_c	critical density (kg m^{-3})
σ	Lennard-Jones diameter (Å)
ε	Lennard-Jones well depth (K)
ε_0	vacuum permittivity (J^{-1} C^2 m^{-1})
η	viscosity (mPa s)
ν_i	stoichiometric coefficient of component *i*
μ_i	chemical potential of component *i* (J)
Γ_i	ratio of experimental over simulated vapour pressures of specie *i*

Acknowledgment

The authors would like to acknowledge the support of the seventh framework program of the European Commission via the collaborative project COCATE "Large-scale CCS Transportation infrastructure in Europe" – GA No. 241381. VL, EB and ND also acknowledge financial help from the French Agence Nationale de la Recherche (ANR), under grant SUSHI (Grant No. ANR-07-BLAN-0268) "SimUlation de Systèmes Hétérogènes et d'Interfaces". BC would like to thank Dr. Bernard Rousseau for the use of the NEWTON MD code.

References

[1] E. de Visser, C. Hendriks, M. Barrio, M. J. Mølnvik,G. de Koeijer, S. Liljemark, Y. Le Gallo, Int. J. Greenhouse Gas Control 2 (2008) 478-487.

[2] H. Li, J.P. Jakobsen, Ø. Wilhelmsen, J. Yan, Appl. Energy 88 (2011) 3567–3579.

[3] H. Li, Ø. Wilhelmsen, Y. Lv, W. Wang, J. Yan, International Journal of Greenhouse Gas Control 5 (2011) 1119–1139.

[4] F. Caubet, Mem. Soc. Sci. Phys. Nat. Bordeaux 3 (1903) 0371-2133.

[5] F. Caubet, Z. Phys. Chem. Stoechiom. Verwandtschaftsl. 49 (1904) 101-116.

[6] D. Cook, Proceedings of the Royal Society of London Series A 219 (1953) 245-256.

[7] J.S. Rowlinson, J.R. Sutton, F. Weston, Proceedings, International Conference Thermodynamics and Transport Properties Fluids, 1957.

[8] C.J. Wormald, J.M. Eyears, J. Chem. Soc. Faraday Trans. I 84 (1988) 3097-3106.

[9] A. Cabanas, J.A.R. Renuncio, C. Pando, Ind. Eng. Chem. Res. 39 (2000) 3566-3575.

[10] J. Kestin, S.T. Ro, Ber. Buns. Phys. Chem. 86 (1982) 948-950.

[11] Ph. Ungerer, B. Tavitian, A. Boutin, Applications of molecular simulation in the oil and gas industry - Monte Carlo methods, Edition Technip, Paris, 2005.

[12] A.Z. Panagiotopoulos, Mol. Phys. 61 (1987) 813-826.

[13] E. Bourasseau, P. Ungerer, A. Boutin, J. Phys. Chem. B 106 (2002) 5483-5491.

[14] M.P. Allen, D.J. Tildesley, Computer simulation of liquids, Oxford Science Publications, Oxford, 1987.

[15] N.T. Van-Oanh, C. Houriez, B. Rousseau, Phys. Chem. Chem. Phys. 12 (2010) 930-936.

[16] C. Nieto-Draghi, A. Bocahut, B. Creton, P. Have, A. Ghoufi, A. Wender, A. Boutin, B. Rousseau, L. Normand, Mol. Sim. 34 (2008) 211-230.

[17] B. Creton, T. de Bruin, V. Lachet, C. Nieto-Draghi, J. Phys. Chem. B 114 (2010) 6522-6530.

[18] C. Nieto-Draghi, T. de Bruin, J. Perez-Pellitero, J. Bonet Avalos, A.D. Mackie, J. Chem. Phys. 126 (2007) 064509.

[19] E. Bourasseau, V. Lachet, N. Desbiens, J.B. Maillet, J.M. Teuler, P. Ungerer, J. Phys. Chem. B 112 (2008) 15783-15792.

[20] V. Lachet, T. de Bruin, P. Ungerer, C. Coquelet, A. Valtz, V. Hasanov, F. Lockwood, D. Richon, Energy Procedia 1 (2009) 1641–1647.

[21] D. Frenkel, B. Smit, Understanding Molecular Simulation. San Diego, Academic Press, 1996.

[22] M.F. Costa Gomes, J. Deschamps, A.A.H. Padua, J. Phys. Chem. B 110 (2006) 18566-18572.

[23] N. Hansen, F.A.B. Agbor, F.J. Keil, Fluid Phase Equil. 259 (2007) 180-188.

[24] M.W. Chase, C.A. Davies, J.R. Downey, D.J. Frurip, R.A. McDonald, A.N. Syverud, J. Phys. Chem. Ref. Data 14 (Suppl. 1), 1985.

[25] Ph. Ungerer, C. Beauvais, J. Delhommelle, A. Boutin, B. Rousseau, A.H. Fuchs, J. Chem. Phys. 112 (2000) 5499-5510.

[26] M.G. Ahunbay, J. Perez-Pellitero, R.O. Conteras-Camacho, J.-M. Teuler, Ph. Ungerer, A.D. Mackie, V. Lachet, J. Phys. Chem. B 109 (2005) 2970-2976.

[27] E. Bourasseau, M. Haboudou, A. Boutin, A.H. Fuchs, Ph. Ungerer, J. Chem. Phys. 118 (2003) 3020-3034.

[28] R.L. Rowley, W.V. Wilding, J.L. Oscarson, N.A. Zundel, T.L. Marshall, T.E. Daubert, R.P. Danner, Design Institute for Physical Properties, AIChE, New York, 2002.

[29] E.L. Quinn, G. Wernimont, J. Am. Chem. Soc. 51 (1929) 2002-2008.

[30] NIST, http://webbook.nist.gov, 2011.

[31] N. Wilding, P. Nielaba, Phys. Rev. 53 (1996) 926-934.

[32] J.L. Barrat, J.P. Hansen, Basic Concepts for simple and Complex liquids, Cambridge University publication, 2003.

[33] A.L. Smith, H.J. Johnston, J. Am. Chem. Soc. 74 (1952) 4696-4698.

[34] H.J.R. Guedes, Thesis, Universidade Nova de Lisboa,1988.

[35] C.E. Dinerman, G.E. Ewing, J. Chem. Phys. 53 (1970) 626-631.

[36] J. Billingsley, A.B. Callear, Trans. Faraday Soc. 67 (1971) 589-597.

[37] E. Forte, H. Van den Bergh, Chem. Phys. 30 (1978) 325-331.

[38] V. Menoux, R. Le Doucen, C. Haeusler, J.C. Deroche, Can. J. Phys. 62 (1984) 322-329.

[39] E.D. Glendening, A.M. Halpern, J. Chem. Phys. 127 (2007) 164307.

[40] K.A. Nguyen, M.S. Gordon, J.A. Montgomery, H.H. Michels, J. Phys. Chem. 98 (1994) 10072-10078.

[41] J.K. Park, H. Sun, Chem. Phys. 263 (2001) 61-68.

[42] F. Kohler, H.J.R. Guedes, J.C. Reves, M. Nunes da Ponte, J. Mol. Liq. 67 (1995) 105-123.

[43] H.J.R. Guedes, M. Nunes da Ponte, High Temp. High Press. 18 (1986) 639-643.

[44] H.L. Johnston, W.F. Giauque, J. Am. Chem. Soc. 51 (1929) 3194-3214.

[45] H.L. Johnston, H.R. Weimer, J. Am. Chem. Soc. 56 (1934) 625-630.

[46] B.H. Golding, B.H. Sage, Ind. Eng. Chem. 43 (1951) 160-161.

[47] A.L. Horvath, Physical Properties of Inorganic Compounds, Crane Russak, New York, 1975.

[48] G.H. Cheesman, J. Chem. Soc. (1932) 889-890.

[49] D.R. Stull, E.F. Jr. Westrum, G.C. Sinke, The Chemical Thermodynamics of Organic Compounds, John Wiley and Sons, New York, 1969.

[50] O.K. Rice, J. Chem. Phys. 4 (1936) 367-372.

[51] C. H. Turner, J. K. Brennan, M. Lísal, W. R. Smith, J. K. Johnson, K. E. Gubbins, Mol. Sim. 34 (2008) 119–146.

[52] W. Smith, B.J. Triska, Chem. Phys. 100 (1994) 3019-3027.

[53] J. Johnson, A. Panagiotopoulos, K. Gubbins, Mol. Phys. 81 (1994) 717-733.

[54] J.O. Hirschfelder, C.F. Curtiss, R.B. Bird, Molecular Theory of Gases and Liquids, Wiley, New York, 1954.

[55] F. Kohler, M. Bohn, J. Fischer, R. Zimmermann, Monatsh. Chem. 118 (1987) 169-182.

[56] J.B. Pedley, Thermodynamical Data and Structures of Organic Compounds, TRC Data Series, Thermodynamic Research Center, College Station: Texas, 1994.

[57] M. Lísal, P. Cosoli, W.R. Smith, S.K. Jain, K.E. Gubbins, Fluid Phase Equil. 272 (2008) 18-31.

[58] E.A. Guggenheim, Mol. Phys. 10 (1966) 401-404.

[59] C.H. Turner, J.K. Johnson, K.E. Gubbins, J. Chem. Phys. 114 (2001) 1851-1859.

[60] J. Harris, K.J. Yung, J. Phys. Chem. 99 (1995) 12021–12024.

[61] M. Lísal, W.R. Smith, I. Nezbeda, J. Phys. Chem. B 103 (1999) 10496-10505.

[62] Ø. Wilhelmsen, G. Skaugen, O, Jørstad, H. Li, Energy Procedia (2012) in press.